IDENTIFYING INTRINSIC CONNECTIVITY NETWORK PATTERNS DURING PROPOFOL-INDUCED LOSS OF CONSCIOUSNESS: A MULTIVARIATE ANALYSIS

Huandong Li[1], Xiaoyuan Liu[2], Nanfeng Jie[1], Maohu Zhu[3], Baoguo Wang[4], Tianzi Jiang[1]

[1]Brainnetome Center, Institute of Automation, Chinese Academy of Sciences, Beijing 100190, China. E-mail: hdli@nlpr.ia.ac.cn
[2]Capital University of Medical Sciences Affiliated Tiantan Hospital, Beijing 100050, China. E-mail: lxy13621278793@163.com.
[3]Elementary Educational College, Jiangxi Normal University, Nanchang 330022, China. E-mail: maohzhu@hotmail.com.
[4]Department of Anesthesiology, Sanbo Brain Hospital, Capital Medical University, Beijing 100093, China. E-mail: wangbg605@sina.com.

Keywords: propofol, functional MRI, SVM-FoBa, feature selection, consciousness

Abstract

Despite the routine use of general anesthesia during surgery, no consensus has been reached on the precise mechanisms by which anesthetic agents suppress consciousness. Recent functional magnetic resonance imaging studies have shown that changes in connectivity is generally observed during propofol-induced loss of consciousness, especially in the fronto-parietal association cortex. Here, we developed a novel feature selection approach based on linear support vector machine with a forward-back search strategy to investigate the mostly discriminative connectivity patterns of different consciousness states. The classification accuracy between wakefulness and deep sedation was up to 96.4%. Weight analysis further revealed that consciousness could be linked to functional connectivity within and across the default mode network, executive control network, salience network and cerebellum. Moreover, the angular, supplementary motor cortex, inferior parietal, insula, and cerebellum exhibited significantly larger weight, suggesting important roles in consciousness. In all, our study sheds light on the mechanism of consciousness.

1 Introduction

Understanding the neurobiological basis of consciousness can bring about a huge impact on science, medicine, and society. Anesthetic agents give us a viable way to study consciousness. Propofol is the most widely used anesthetic agent in clinic procedures, characterized by dose-related impairment of cognition and consciousness. However, the mechanism by which propofol functions is not yet fully acknowledged. Hence, to better understand the neurobiological basis of consciousness, more attention on this topic is urgently needed.

At a small dose, propofol first suppresses thinking and focused attention. Reduced functional connectivity in the default mode network (DMN) was generally observed. However, intrinsic activities were relatively preserved [8, 10, 13]. As the dose is increased, functional connectivity in the fronto-parietal network is often reduced, which suggests that propofol breaks functional information integration by disrupting the interaction of the sensory information and high-order processing cortex [2, 11, 14]. At an even higher dose, brain activity is widely suppressed, while mainly mediating at the brainstem and spinal levels [3, 9].

In recent years, increased attention has been given to large-scale neural network functions, referred to here as intrinsic connectivity networks (ICNs), with distinct functions such as vision, hearing, sensorimotor, attention, working memory, and salience processing [6]. Previous studies concerning ICNs during altered consciousness have demonstrated that high-order ICNs (e.g., default mode network, salience network, and executive control network) decreased in connectivity when consciousness is reduced [2, 9, 14, 18].

The results mentioned above were mostly detected by univariate approaches. These studies provide valuable insight into the mechanism of consciousness. However they also have significant limitations because they ignore the fact that the brain actually functions in a multivariate way [12]. On the other hand, multivariate pattern analysis is increasingly used based on functional MRI data [7, 17, 20]. This method can complement both seed-based and univariate statistical analysis. Recently, Shirer et al. distinguished specific cognitive states with intrinsic connectivity patterns using a multivariate pattern analysis [15].

Therefore, the present study sought to classify different states of consciousness using intrinsic network patterns and to identify the related features in order to explain altered states of consciousness.

2 Materials and methods

2.1 Participants

Sixteen (8 male; age range, 18-39 year; mean age ± SD, 25.3 ± 7.4 year; weight range, 48-75 kg; mean weight ± SD, 58 ± 8 kg) right-handed normal participants were recruited by local advertisement. All subjects had no history of psychiatric or neurological illness, psychiatric treatment, or drug addiction.

The research was approved by the Medical Research Ethics Committee of Tiantan Hospital and all of the subjects gave written informed consent.

2.2 Sedation protocol

Subjects fasted for at least 6 hours from solids and 4 hours from liquids before sedation. Propofol was administrated with target controlled infusion (TCI) by using a TCI pump (Base Primea Orchestra Workstation, Fresenius SE & Co. KGaA) coupled with the assessment of OAA/S (observer's assessment of alertness/sedation) scores. Light sedation was induced to achieve a plasma concentration of 1.0 μg/ml and deep sedation was induced to achieve a concentration of 3.0 μg/ml. Once a desired sedation state was reached and kept stable for another 10 minutes, the level of consciousness was clinically evaluated using the OAA/S scores, and fMRI scans were performed subsequently for ~5 minutes. Electrocardiogram (ECG), blood pressure (MAP), pulse oxymetry (SpO2) and end-tidal carbon dioxide (etCO2) were continuously monitored throughout the experiment. A summary of the physiological measurements is presented in Table 1.

2.3 MR data acquisition

All MR images were acquired on a 3.0 Tesla scanner (Magnetom Trio, Siemens, Erlangen, Germany). The blood oxygenated level-dependent (BOLD) images of the whole brain were acquired using an echo-planar imaging sequence (TR/TE = 2000/30 ms; FA = 90°; FOV = 256 mm × 256 mm; matrix size = 64 × 64; slice thickness/gap = 4.0/0.0 mm; voxel size = 4.0mm × 4.0mm × 4.0 mm; 32 transversal slices; 150 volumes). The fMRI scan were repeated during each clinical state. Additionally, a high resolution T1-weighted image was also performed for each volunteer in this study.

2.4 Data preprocessing

The fMRI data was preprocessed using the Data Processing Assistant for Resting-State fMRI (DPARSF) [5]. After discarding the first 5 volumes of each session to allow for magnetization equilibrium, the following steps were performed: realigning images to the first volume; co-registering the structural volume to the mean functional image; removing the linear trend; regressing nuisance signals (6 motion parameters, global mean signal and average BOLD signal in white matter and CSF); temporal filtering (0.01-0.1 Hz), normalizing the anatomy volume to the MNI152 standard template; resampling the functional data to MNI space with the concatenated transformations, and spatial smoothing with a 6-mm full-width at half-maximum Gaussian kernel. Two volunteers did not finish the fMRI scanning at deep sedation and two subjects had excessive head movements. In total, the sample size of participants while awake, at light, and during deep levels of sedation was 15, 16 and 13, respectively.

2.5 ROI and functional connectivity matrix creation

First of all, we performed the ICA using FSL's MELODIC software (http://fsl.fmrib.ox.ac.uk/fsl/fslwiki/MELODIC) on the group-level resting-state data for all subjects in the wakefulness condition and obtained 30 components. Ten meaningful components were identified visually as being ICNs based on previous reports [1, 6, 15, 16, 19], including the anterior default mode network (aDMN), posterior default mode network (pDMN), left executive control network (LECN), right executive control network (RECN), task-positive network (TPN), language network (LN), salience network (SN), sensorimotor network (SMN), auditory network (AN) and visual network (VN). Cortical representation of these ICNs are shown in Figure 1. Each of the ICNs was thresholded to get distinct moderately sized clusters. Then, we defined ROIs as spherical regions with a radius of 6 mm at the centre of the peak coordinates of the obtained clusters. This step resulted in 48 ROIs (Figure 2). We calculated the Pearson's correlation coefficient between the time series of all ROIs for each subject in wakefulness and the two sedation states.

2.6 Development of SVM-FoBa

Considering the computational advantage, greed search strategies generally serve in two directions: forward selection and backward elimination. Forward selection is a bottom-up analogy that starts with en empty set. In each iteration step, one feature is added to the current set F to reduce the loss function J. However, forward selection will yield nested sets of features, as features selected at step k are always included in the subset of step $(k+1)$. On the other hand, backward elimination is a top-down search model that starts with the complete set, removing one feature at a time so that the negative impact on performance would be kept minimal until the change of loss function J exceeds a certain threshold. Therefore, backward elimination also generates nested subsets. What's more, a major flaw of backward elimination is the propensity for overfitting.

In a word, both forward and backward strategies have their disadvantages. However, if we combined the forward selection with backward elimination, the error induced by the earlier steps may be adaptively corrected. Hence, we developed "SVM-FoBa", a SVM-based adaptive forward-backward greedy algorithm. It is defined as follows: Assuming that a feature i_k is added to the feature subset F_{k-1} by a forward step at stage k, a subset of F_k is generated, with J_k being the corresponding value of the optimization objective function. The decrement of the objective function is denoted as δ_k^+, so that $\delta_k^+ = J_{k-1} - J_k$. The backward step then locates a feature $j_k \in F_k$, whose elimination induces the smallest increment in the objective function, denoted as δ_k^-. If $\delta_k^- < 0.5\,\delta_k^+$, we define that at least one error has occurred in the earlier forward steps.

Once errors induced by the earlier forward steps are detected, backward elimination processes will automatically step in and repeat until all the errors are corrected. The pseudo-code for SVM-FoBa is demonstrated in Figure 3. In this study, we invoked the value of the optimization objective function of the linear SVM as the loss function J and adapted LibSVM [4] with SVM-FoBa algorithm to accomplish the feature selection.

Parameter	Wakefulness	Light Sedation	Deep Sedation
MAP (mmHg)	88 ± 8	82 ± 8	75 ± 7
HR (bpm)	66 ±9	64 ± 7	68 ± 8
SpO2 (%)	100 ± 0	99 ± 1	98 ± 2
EtCO2 (%)	38.1 ± 2.4	38.9 ± 2.1	44.3± 2.7
OAA/S	5 ± 0	4 ± 0.2	2 ± 0.4

Table 1: Physiological variables and OAA/S scores
Results are expressed as mean ± standard deviation of individual values in each state.

3 Results

3.1 Physiological variables

Physiological variables did not change significantly in the awake, light sedation, or deep sedation states. The OAA/S scores gradually decreased with increasing doses of propofol (Table 1).

3.2 Comparison with typical feature selection methods

To validate the effectiveness of SVM-FoBa, we tested different feature selection methods on public data sets. Besides SVM-FoBa, three types of conventional feature selection methods were chosen, including the univariate T-test, Fisher score ranking and forward selection approach. For each method, we conducted a linear SVM binary classifier for performance evaluation.
Due to our limited number of samples, public data sets with an approximate number of instances were intentionally chosen for the binary classification test. We used a leave-one-out cross-validation strategy to estimate the generalization ability of classifiers. Detailed information and results are given in Table 2.
As a general rule, SVM-FoBa outperformed traditional feature selection methods in the comparison study, though the T-test ranking and Fisher score ranking performed similarly to SVM-FoBa on the "DBWorld e-mails" data set.

3.3 Classification results

We performed three binary classification tasks: wakefulness vs. light sedation, light sedation vs. deep sedation, and wakefulness vs. deep sedation. For each task, the former type was the negative class, while latter was the positive class. The highest accuracy rate reached 96.43% for wakefulness vs. deep sedation. In other words, only one subject in the deep sedation group was misclassified. Furthermore, the accuracy rate was minimum for wakefulness vs. light sedation (see Table 3 for details). Obviously, the differences in intrinsic network patterns between wakefulness and deep sedation were mostly stable and significant.

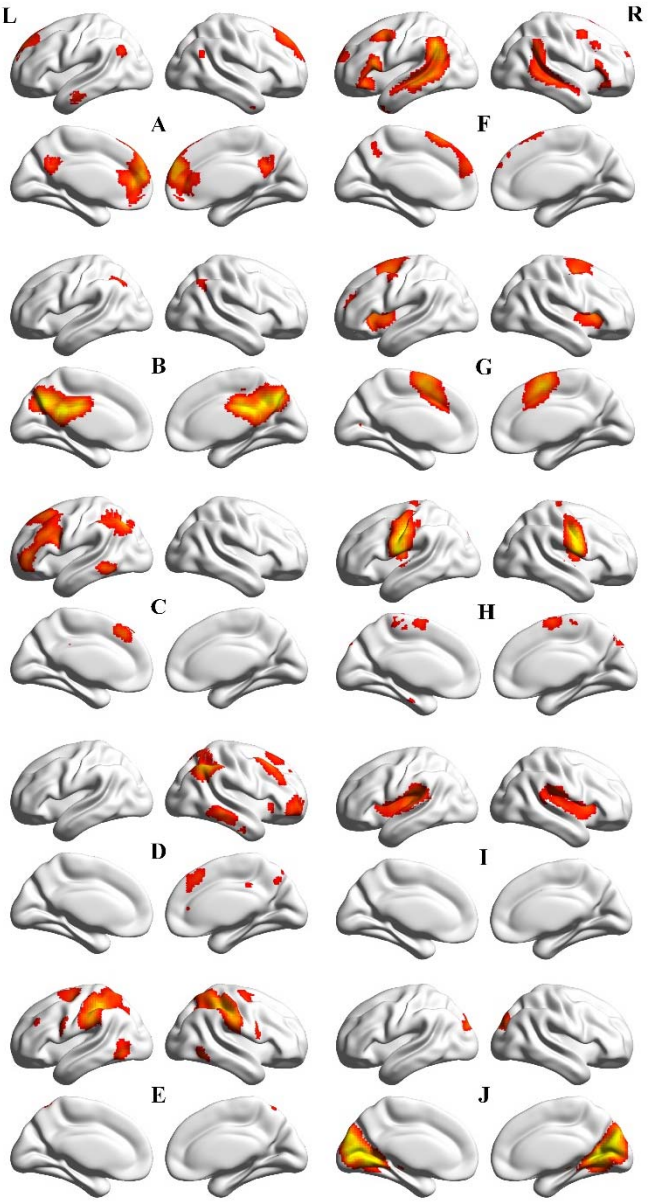

Figure 1: Ten ICNs from the 30-components analysis of the subjects in normal awake state. ICNs are displayed on a surface of the brain (Brainnet View). (A) aDMN; (B) pDMN; (C) LECN; (D) RECN; (E) TPN; (F) LN; (G) SN; (H) SMN; (I) (AN); (J) VN.

3.4 Altered resting-state functional connectivity during propofol-induced loss of consciousness

In addition to classification accuracy, we were more interested in which functional connections contributed most to group discrimination. This was done by exploiting the quantitative advantage of the linear SVM classification model, while features having the greatest absolute weight could be found out. We denoted such important features as the "discriminant

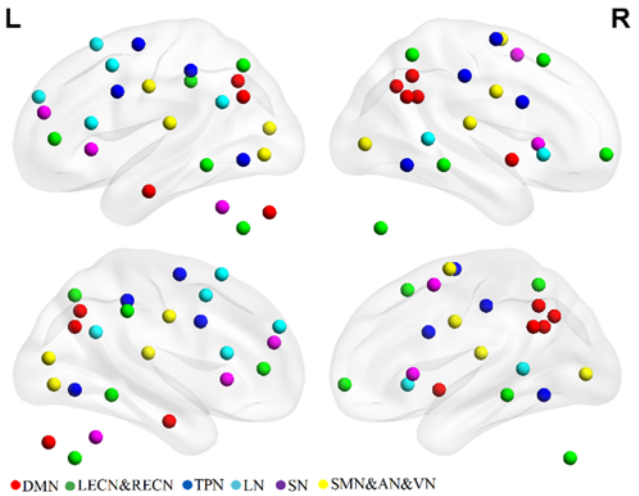

Figure 2: 48 ROIs defined from 10 ICNs.

Start with the feature set $F = \emptyset$

Forward loop (Step n)

Add one feature to F that maximizes $\delta_n^+ = J_{n-1} - J_n$

Backward loop (Step k)

Delete one feature from F that minimizes $\delta_k^- = J_k^- - J_n$

Stop when $\delta_k^- > \frac{\delta_n^+}{2}$

Stop when $\delta_n^+ < \varepsilon$

Output F

Figure 3: Pseudo-code for SVM-FoBa algorithm

features". (1) The discriminant features were mostly located between DMN, SN, and SMN for the wakefulness classification with light sedation. (2) Functional connectivity within DMN, and DMN connectivity with SN and ECN, were changed from light sedation to deep sedation. (3) Functional connectivity within and across DMN, SN, and ECN contributed the most for wakefulness vs. deep sedation. Several regions exhibited great weights (1/2 the sum of the absolute weights of all the connections to and from that ROI), i.e. SMA, cerebellum, insula, inferior parietal, prefrontal cortex, and post cingulate cortex in distinguishing states of consciousness (Figure 4).

4 Discussion and conclusion

As far as we know, this study is the first to employ the pattern-classification method in order to discriminate different states of consciousness induced by propofol. Brain function during light sedation was mainly preserved so that the discrimination of wakefulness and light sedation was the lowest. The accuracy reached 96.4% for wakefulness vs. deep sedation. Intuitively, there were stable and significant differences between wakefulness and deep sedation. Weight analysis of the selected features further revealed that propofol-induced loss of consciousness could be linked to the reconfiguration of large-scale brain intrinsic networks. The regions with high discriminative powers were SMA, cerebellum, insula, inferior parietal, prefrontal cortex, and post cingulate cortex, indicating that these regions may play important roles in the neurobiological basis of consciousness.

DBWorld e-mails	**64 instances**		**4,702 features**	
Method	Accuracy	Sensitivity	Specificity	No.features
SVM-FoBa	**90.63**	**84.21**	**89.66**	**73-84**
Forward	85.94	88.57	82.76	1-3
T-test	90.63	84.21	89.66	73-84
Fisher score	90.63	84.21	89.66	73-84
Colon Cancer	**62 instances**		**2,000 features**	
Method	Accuracy	Sensitivity	Specificity	No.features
SVM-FoBa	**87.10**	**92.50**	**86.36**	**29-30**
Forward	87.10	92.50	81.82	4
T-test	85.48	87.50	86.36	29-30
Fisher score	87.10	87.50	86.36	29-30
Leukemia Cancer	**72 instances**		**7,129 features**	
Method	Accuracy	Sensitivity	Specificity	No.features
SVM-FoBa	**98.61**	**96.00**	**100**	**30-38**
Forward	95.83	96.00	100	2-3
T-test	95.83	96.00	95.74	30-38
Fisher score	95.83	96.00	95.74	30-38

Table 2: Performance comparison (%) among different feature selection methods on three public data sets T-Test and Fisher score use the same number of features with that of SVM-FoBa for equivalent comparisons. "73-84" means equal performance from 73 to 84 features. The "DBWorld e-mails" data set was obtained from UCI Machine Learning Repository at http://archive.ics.uci.edu/ml; also, descriptions of "Leukemia Cancer" and "Colon Cancer" can be found at http://www.inf.ed.ac.uk/teaching/courses/dme/html/datasets0405.html.

rs-fMRI FC	**1128 features**		
	Awake *vs.* Light	Light *vs.* Deep	Awake *vs.* Deep
Accuracy	**74.19%**	**86.21%**	**96.43%**
Sensitivity	73.33%	87.50%	100%
Specificity	75.00%	84.62%	92.31%
No. features	13	10-11	18-19

Table 3: Classification results of SVM-FoBa using the functional connectivity matrix. The accuracy rates were calculated by dividing the number of the correct predictions across all folds of LOOCV by the number of samples. The sensitivity and specificity were obtained likewise.

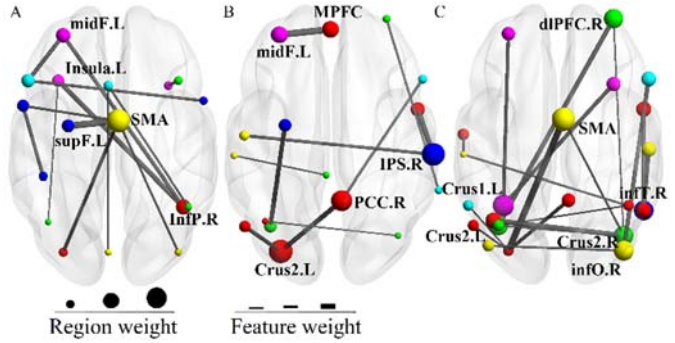

Figure 4: Axial view of the most discriminating functional connections and regions. (A) 13 most weight features identified for wakefulness vs. light sedation. (B) 10 most weight features identified for light sedation vs. deep sedation. (C) 18 most weight features identified for wakefulness vs. deep sedation. Regions are color-code by network.

References

[1] C. F. Beckmann, and S. M. Smith. "Tensorial extensions of independent component analysis for multisubject FMRI analysis", *Neuroimage,* vol. 25, no. 1, pp. 294-311, 2005.

[2] P. Boveroux, A. Vanhaudenhuyse, M. A. Bruno, Q. Noirhomme, S. Lauwick, A. Luxen, C. Degueldre, A. Plenevaux, C. Schnakers, C. Phillips, J. F. Brichant, V. Bonhomme, P. Maquet, M. D. Greicius, S. Laureys, and M. Boly. "Breakdown of within- and between-network resting state functional magnetic resonance imaging connectivity during propofol-induced loss of consciousness", *Anesthesiology,* vol. 113, no. 5, pp. 1038-1053, 2010.

[3] J. A. Campagna, K. W. Miller, and S. A. Forman. "Mechanisms of actions of inhaled anesthetics", *N Engl J Med,* vol. 348, no. 21, pp. 2110-2124, 2003.

[4] Y. Chao-Gan, and Z. Yu-Feng. "DPARSF: A MATLAB Toolbox for "Pipeline" Data Analysis of Resting-State fMRI", *Front Syst Neurosci,* vol. 4, pp. 13, 2010.

[5] J. S. Damoiseaux, S. A. Rombouts, F. Barkhof, P. Scheltens, C. J. Stam, S. M. Smith, and C. F. Beckmann. "Consistent resting-state networks across healthy subjects", *Proc Natl Acad Sci U S A,* vol. 103, no. 37, pp. 13848-13853, 2006.

[6] N. U. Dosenbach, B. Nardos, A. L. Cohen, D. A. Fair, J. D. Power, J. A. Church, S. M. Nelson, G. S. Wig, A. C. Vogel, C. N. Lessov-Schlaggar, K. A. Barnes, J. W. Dubis, E. Feczko, R. S. Coalson, J. R. Pruett, Jr., D. M. Barch, S. E. Petersen, and B. L. Schlaggar. "Prediction of individual brain maturity using fMRI", *Science,* vol. 329, no. 5997, pp. 1358-1361, 2010.

[7] M. D. Greicius, V. Kiviniemi, O. Tervonen, V. Vainionpaa, S. Alahuhta, A. L. Reiss, and V. Menon. "Persistent default-mode network connectivity during light sedation", *Hum Brain Mapp,* vol. 29, no. 7, pp. 839-847, 2008.

[8] P. Guldenmund, A. Demertzi, P. Boveroux, M. Boly, A. Vanhaudenhuyse, M. A. Bruno, O. Gosseries, Q. Noirhomme, J. F. Brichant, V. Bonhomme, S. Laureys, and A. Soddu. "Thalamus, brainstem and salience network connectivity changes during propofol-induced sedation and unconsciousness", *Brain Connect,* vol. 3, no. 3, pp. 273-285, 2013.

[9] S. G. Horovitz, M. Fukunaga, J. A. de Zwart, P. van Gelderen, S. C. Fulton, T. J. Balkin, and J. H. Duyn. "Low frequency BOLD fluctuations during resting wakefulness and light sleep: a simultaneous EEG-fMRI study", *Hum Brain Mapp,* vol. 29, no. 6, pp. 671-682, 2008.

[10] X. Liu, K. K. Lauer, B. D. Ward, S. M. Rao, S. J. Li, and A. G. Hudetz. "Propofol disrupts functional interactions between sensory and high-order processing of auditory verbal memory", *Hum Brain Mapp,* vol. 33, no. 10, pp. 2487-2498, 2012.

[11] K. A. Norman, S. M. Polyn, G. J. Detre, and J. V. Haxby. "Beyond mind-reading: multi-voxel pattern analysis of fMRI data", *Trends Cogn Sci,* vol. 10, no. 9, pp. 424-430, 2006.

[12] M. S. Schroter, V. I. Spoormaker, A. Schorer, A. Wohlschlager, M. Czisch, E. F. Kochs, C. Zimmer, B. Hemmer, G. Schneider, D. Jordan, and R. Ilg. "Spatiotemporal reconfiguration of large-scale brain functional networks during propofol-induced loss of consciousness", *J Neurosci,* vol. 32, no. 37, pp. 12832-12840, 2012.

[13] J. Schrouff, V. Perlbarg, M. Boly, G. Marrelec, P. Boveroux, A. Vanhaudenhuyse, M. A. Bruno, S. Laureys, C. Phillips, M. Pelegrini-Issac, P. Maquet, and H. Benali. "Brain functional integration decreases during propofol-induced loss of consciousness", *Neuroimage,* vol. 57, no. 1, pp. 198-205, 2011.

[14] W. R. Shirer, S. Ryali, E. Rykhlevskaia, V. Menon, and M. D. Greicius. "Decoding subject-driven cognitive states with whole-brain connectivity patterns", *Cereb Cortex,* vol. 22, no. 1, pp. 158-165, 2012.

[15] S. M. Smith, P. T. Fox, K. L. Miller, D. C. Glahn, P. M. Fox, C. E. Mackay, N. Filippini, K. E. Watkins, R. Toro, A. R. Laird, and C. F. Beckmann. "Correspondence of the brain's functional architecture during activation and rest", *Proc Natl Acad Sci U S A,* vol. 106, no. 31, pp. 13040-13045, 2009.

[16] X. Song, and N. K. Chen. "A SVM-based quantitative fMRI method for resting-state functional network detection", *Magn Reson Imaging,* vol. 32, no. 7, pp. 819-831, 2014.

[17] G. Tononi. "An information integration theory of consciousness", *BMC Neurosci,* vol. 5, pp. 42, 2004.

[18] D. Wang, W. Qin, Y. Liu, Y. Zhang, T. Jiang, and C. Yu. "Altered resting-state network connectivity in congenital blind", *Hum Brain Mapp,* vol. 35, no. 6, pp. 2573-2581, 2014.

[19] L. L. Zeng, H. Shen, L. Liu, L. Wang, B. Li, P. Fang, Z. Zhou, Y. Li, and D. Hu. "Identifying major depression using whole-brain functional connectivity:

a multivariate pattern analysis", *Brain,* vol. 135, no. Pt 5, pp. 1498-1507, 2012.